

RL-TR-91-341  
Final Technical Report  
December 1991

AD-A246 369



2

# HIGH-SPEED PULSE DETECTION ROOM- TEMPERATURE OPTICAL NONLINEARITIES FOR GaInAs/A1InAs AND GaA1InAs/A1InAs MULTIPLE QUANTUM WELLS AND INTEGRATED MIRROR ETALON AT 1.3 $\mu$ m

University of Arizona

N.Peyghambarian, Steven T. Johns, Mark F. Krol,  
John L. Stacy, Raymond K. Boncek

DTIC  
ELECTE  
FEB 21 1992  
S D D

*APPROVED FOR PUBLIC RELEASE; DISTRIBUTION UNLIMITED.*

92-03843



Rome Laboratory  
Air Force Systems Command  
Griffiss Air Force Base, NY 13441-5700

92 2 13 111

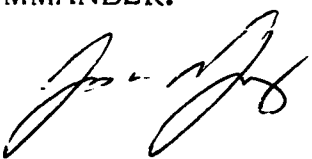
This report has been reviewed by the Rome Laboratory Public Affairs Office (PA) and is releasable to the National Technical Information Service (NTIS). At NTIS it will be releasable to the general public, including foreign nations.

RL-TR-91-341 has been reviewed and is approved for publication.

APPROVED:

  
STEVEN T. JOHNS  
Project Engineer

FOR THE COMMANDER:

  
JAMES W. YOUNGBERG, LT COL, USAF  
Deputy Director  
Surveillance and Photonics Directorate

If your address has changed or if you wish to be removed from the Rome Laboratory mailing list, or if the addressee is no longer employed by your organization, please notify RL(OCPA), Griffiss AFB NY 13441-5700. This will assist us in maintaining a current mailing list.

Do not return copies of this report unless contractual obligations or notices on a specific document require that it be returned.

# REPORT DOCUMENTATION PAGE

Form Approved  
OMB No. 0704-0188

Public reporting burden for this collection of information is estimated to average 1 hour per response, including the time for reviewing instructions, searching existing data sources, gathering and maintaining the data needed, and completing and reviewing the collection of information. Send comments regarding this burden estimate or any other aspect of this collection of information, including suggestions for reducing this burden, to Washington Headquarters Services, Directorate for Information Operations and Reports, 1215 Jefferson Davis Highway, Suite 1204, Arlington, VA 22202-4302, and to the Office of Management and Budget, Paperwork Reduction Project (0704-0188), Washington, DC 20503.

1. AGENCY USE ONLY (Leave Blank)		2. REPORT DATE December 1991		3. REPORT TYPE AND DATES COVERED Final Dec 89 - Jul 91	
4. TITLE AND SUBTITLE HIGH-SPEED PULSE DETECTION ROOM-TEMPERATURE OPTICAL NONLINEARITIES FOR GaInAs/AlInAs AND GaAlInAs/AlInAs MULTIPLE QUANTUM WELLS AND INTEGRATED MIRROR ETALON AT 1.3um				5. FUNDING NUMBERS C - F30602-88-D-0026, 0024 PE - 62702F PR - 4600 PA - P2	
6. AUTHOR(S) N. Peyghambarian, Steven T. Johns, Mark F. Krol, John L. Stacy, Raymond K. Boncek					
7. PERFORMING ORGANIZATION NAME(S) AND ADDRESS(ES) University of Arizona Optical Sciences Center Tucson, AZ 85721				8. PERFORMING ORGANIZATION REPORT NUMBER	
9. SPONSORING/MONITORING AGENCY NAME(S) AND ADDRESS(ES) Rome Laboratory (OCA) Griffiss AFB NY 13441-5700				10. SPONSORING/MONITORING AGENCY REPORT NUMBER RL-TR-91-341	
11. SUPPLEMENTARY NOTES RL Project Engineer: Steven T. Johns/RL/OCA/(315)330-4456 Prime Contractor: Calspan-UB Research Center, P.O. Box 400, Buffalo, NY 14225					
12a. DISTRIBUTION/AVAILABILITY STATEMENT Approved for public release; distribution unlimited				12b. DISTRIBUTION CODE	
13. ABSTRACT (Maximum 200 words)  The room-temperature nonlinear absorption spectra of a 40 A GaInAs/AlInAs and a 90 A GaAlInAs/AlInAs multiple quantum well (MQW) were measured near 1.3um using a pump and probe technique. Saturation carrier densities at the heavy-hole exciton peak were determined to be $1.2 \times 10^{18}$ and $1.0 \times 10^{18} \text{ cm}^{-3}$ with a carrier recovery times of $\approx 5\text{ns}$ and $\approx 750 \text{ ps}$ for the two samples, respectively. These measured saturation carrier densities are close to the reported values for GaAs/AlGaAs MQWs. Fabry-Perot etalons with integrated mirrors grown by molecular beam epitaxy (MBE) with GaInAs/AlInAs MQWs as spacer layers were also fabricated as optical logic gate devices. We demonstrated a 125 ps recovery time for the etalon switching device at room temperature.					
14. SUBJECT TERMS Nonlinear Absorption, Multiple Quantum Well (MQW), Exciton				15. NUMBER OF PAGES 40	
				16. PRICE CODE	
17. SECURITY CLASSIFICATION OF REPORT UNCLASSIFIED	18. SECURITY CLASSIFICATION OF THIS PAGE UNCLASSIFIED	19. SECURITY CLASSIFICATION OF ABSTRACT UNCLASSIFIED	20. LIMITATION OF ABSTRACT UL		

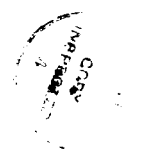
## Table of Contents

1. Abstract . . . . .	3
2. Introduction . . . . .	4
3. Nonlinear Mechanisms in the Bulk Semiconductors Near the Band-Gap . . . . .	6
4. Excitonic Optical Nonlinearities in MQW Structures . . . . .	8
5. Room-Temperature Optical Nonlinearities of GaInAs/AlInAs and GaAlInAs/AlInAs MQWs at 1.3 $\mu\text{m}$ . . . . .	10
6. Nonlinear Fabry-Perot Etalon . . . . .	15
7. Design and Fabrication . . . . .	16
8. The Recovery Time Measurements of Integrated Mirror Etalons at 1.3 $\mu\text{m}$ . . . . .	19
9. Conclusions . . . . .	20
10. Future Work . . . . .	20
11. Figure Illustrations . . . . .	21
12. References . . . . .	32

## Abstract

The room-temperature nonlinear absorption spectra of a 40 Å GaInAs/AlInAs and a 90 Å GaAlInAs/AlInAs multiple quantum well (MQW) were measured near 1.3 μm using a pump and probe technique. Saturation carrier densities at the heavy-hole exciton peak were determined to be  $1.2 \times 10^{18}$  and  $1.0 \times 10^{18} \text{ cm}^{-3}$  with carrier recovery times of  $\approx 5 \text{ ns}$  and  $\approx 750 \text{ ps}$  for the two samples, respectively. These measured saturation carrier densities are close to the reported values for GaAs/AlGaAs MQWs. Fabry-Perot etalons with integrated mirrors grown by molecular beam epitaxy (MBE) with GaInAs/AlInAs MQWs as spacer layers were also fabricated as optical logic gate devices. We demonstrated a 125 ps recovery time for the etalon switching device at room temperature.

Accession For	
NTIS CRA&I	<input checked="checked" type="checkbox"/>
DTIC TAB	<input type="checkbox"/>
Unannounced	<input type="checkbox"/>
Justification	
By	
Distribution /	
Availability Codes	
Dist	Avail and/or Special
A-1	



## Introduction

As a result of the advances in optical fiber communication technology, the dream of a high bit-rate telecommunication system now becomes possible. However, the performance of optical fiber communication systems is limited due to the lack of a high speed signal processor to process the information. At present, the processing speed of an optical fiber communication system is determined by the speed of an electronic logic gate. Currently, the switching times of an electronic transistor is usually in 0.1 ns to 1 ns range and this switching speed is already approaching some of its fundamental limits [Keyes (1981)]. On the other hand, optical switching devices have been shown exhibit sub-picosecond switching speeds [Hulin *et al.*(1986), Friberg *et al.* (1987)], so photonic processing is an alternative technology of processing signals in optical fiber communication systems. Photonic processing also has the potential to avoid the optical-electronic conversion which is used now in the telecommunication system.

The optical time-division multiplexing technique is an extension of the well-known electronic multiplexing technique. In an optical time-division multiplexing system, a high bit-rate data stream is constructed directly by time-multiplexing several lower bit-rate signals. Similarly, at the receiver end of the system, the very high bit-rate optical signal is demultiplexed to several lower bit-rate optical signals before detection and conversion to the electronic domain [Tucker *et al.* (1988)]. Generally, a high bit-rate system requires a high speed signal processor to demultiplex the high bit-rate data. For a 10 Gbit/sec system, the optical switching device must have a high switching contrast and a switching speed faster than 100 picoseconds of full recovery time [Johns (1991)]. In this research, nonlinear Fabry-Perot etalons are being studied as a possible high speed photonic switching device.

The operating wavelength of optical switching devices should match the optical wavelength used in optical fiber communication systems. The proper operating wavelength of an optical switching device in an optical fiber communication system is near 1.3  $\mu\text{m}$  or 1.5  $\mu\text{m}$ , because optical fibers have the smallest absorption and group velocity dispersion in these wavelength

regions [Senior (1985)]. Generally, the operating mechanism of optical switching devices utilizes the nonlinear optical effects of the materials in the devices, so it is clear that the nonlinear optical materials should have large optical nonlinearities and fast response times in the operating wavelength. Because semiconductor materials usually exhibit large optical nonlinearities in the vicinity of the absorption band-edge due to resonance effects, the best materials for optical switching devices in optical fiber communication systems should have absorption band-edges in the  $1.3\ \mu\text{m}$  or  $1.5\ \mu\text{m}$  regions. GaInAs and its related materials have this property. In order to design a practical nonlinear optical switching device for optical fiber communication systems, it is crucially important to understand the nonlinear optical properties of GaInAs and related materials.

Recent advances in crystal growth techniques such as molecular beam epitaxy (MBE) and metalorganic chemical vapor deposition (MOCVD) allow the growth of high quality multiple quantum well (MQW) crystals of precise layer thickness. Due to the quantum confinement effect in semiconductor MQWs, the linear and nonlinear optical properties of MQWs are different from those of bulk semiconductors (we will discuss this later). In general, MQWs have larger optical nonlinearities than bulk materials [Park *et al.* (1988)] and studies of the nonlinear optical properties in MQWs are important in developing a practical nonlinear switching device.

In this manuscript, the nonlinear optical properties near the absorption edge for both bulk and MQW semiconductors will be reviewed and the room-temperature optical nonlinearities of GaInAs/AlInAs and GaAlInAs/AlInAs MQWs at  $1.3\ \mu\text{m}$  will be presented. We will also examine a nonlinear optical Fabry-Perot (FP) etalon of GaInAs/AlInAs MQWs as an example of a photonic switching device for optical fiber telecommunication systems. The basic theory of the operation for a nonlinear optical FP etalon will be introduced, then the design and fabrication of GaInAs/AlInAs MQW nonlinear optical FP etalons will be discussed. In the last section, the recovery time of GaInAs/AlInAs etalons will be reported.

## Nonlinear Mechanisms in the Bulk Semiconductors Near the Band-Gap

The carrier density dependent nonlinear optical effects of semiconductor materials have been studied extensively for potential applications in opto-electronic and all-optical devices [Haug (1988), Gibbs *et al.* (1990)], since there are large optical nonlinearities in the vicinity of their band-edge. The carrier density dependent nonlinear optical effects in semiconductors are due to the interaction between laser light and the material. Most nonlinear effects depend on the intensity of the incident laser light. As laser light is absorbed by semiconductors, electrons and holes are generated in the conduction band and the valence band, respectively. An electron in the conduction band and a hole in the valence band are attracted to each other by the Coulomb force and form bound states. This hydrogen-like electron-hole pair is called an exciton. Excitons have binding energies and Bohr radii like a hydrogenic system, and the binding energy is inversely proportional to the Bohr radius. Normally there are two kinds of excitons. In the first type, named Wannier excitons, the Bohr radius is comparable to the length of the lattice unit cell and this is usually true for III-V and II-VI semiconductors. In the second type, named Frenkel excitons the Bohr radius is on the order of or smaller than an atomic unit cell which is true in some organic materials [Knox (1963), Cho (1979)]. Here we will focus our attention on the Wannier excitons. It is well known that Wannier excitons play an important role in the linear and nonlinear optical properties of semiconductors [Chemla and Miller (1985), Peyghambarian *et al.* (1988)]. The Coulomb interaction between the excited electrons and holes significantly changes the linear absorption spectrum of bulk semiconductors from a basic non-interacting approximation. The major differences of the absorption spectrum, as shown in Fig. 1, are the appearance of discrete (excitonic) lines below the band-gap and the enhancement of absorption above the band-gap (Coulomb enhancement) [Elliot (1957), Bassani (1975), Banyai and Koch (1986)]. However, the excitonic features can not be observed in room temperature experiments because of the scattering of electron-hole pairs by phonons.

Generally, there are two categories of optical nonlinearities in semiconductors: quasi-equilibrium and transient nonlinearities. Quasi-equilibrium nonlinearities are mainly due to the



real carriers, which are generated by resonance or above band-gap photo-excitation. The life-time of quasi-equilibrium nonlinearities is determined by the life-time of carriers but not by the laser pulse duration. Once carriers are generated from photo-excitation, the bound electron and hole pairs collide with each other and with other excitations in the solid such as phonons on a time scale of the order of a few hundred femtoseconds [Chemla *et al.* (1984)]. After these collisions, the carriers are in thermal equilibrium within each band, but not in thermal equilibrium with the whole semiconductor. The electrons in the conduction band will return to the valence band on a time scale of nanoseconds either by radiative or nonradiative processes, and then the whole semiconductor will be in thermal equilibrium. Typically, the life-time of quasi-equilibrium nonlinearities in semiconductors is on the order of nanoseconds because the life-time of the carriers is on the order of nanoseconds. In contrast, for the transient nonlinearities, the optical nonlinear effects do not depend on real carrier generation [Haug (1988), Lee *et al.* (1991)]. The life-time of this nonlinearity follows the excitation laser pulse time profile and is limited by the dephasing time of the electronic resonance. The laser frequency is often tuned below the exciton resonance into the transparency region of the semiconductor so that real carrier generation is minimized. Throughout the following discussions of optical nonlinearities of semiconductors, we will concentrate on the quasi-equilibrium case.

The microscopic origins of the nonlinear optical effects in semiconductors are explained theoretically by many-body effects [Huang (1988), Banyai and Koch (1986)], which take into account the complicated interactions between the electron-hole pairs resulting from the large carrier concentration. Various nonlinear mechanisms such as bandfilling, bandgap renormalization, and Coulomb screening will be discussed.

The Pauli exclusion principle permits only one fermion in the same quantum state, and this introduces the band filling effect. If the allowed electron and hole states are occupied, further transitions into those states are prohibited. As the electron states near the bottom of the conduction band and the hole states near the top of valence band are filled, the photon energy needed for further transitions is increased, resulting in a bleaching of the absorption in the vicinity of the band-gap and it appears as if the absorption edge is shifted to the high energy

side.

The band-gap renormalization is also a consequence of the many-body effect. The two main mechanisms which govern renormalization are the intraband Coulomb repulsion between like charges and the exchange interactions between identical particles. The net result reduces the spatial correlation of the electrons and therefore reduces the overall system energy [Haug and Schmitt-Rink (1985)]. The band-gap renormalization results in a red shift of absorption band-edge.

As the photo-generated carrier density becomes large, the Coulomb interaction between an electron and a hole decreases as a result of the screening effect of other nearby charged carriers. The screened Coulomb potential between an electron and a hole is weaker than the unscreened potential and decreases exponentially for large separations between charges. This screening effect reduces the binding energy of the excitons. As the screening increases, the Bohr radius of the exciton increases and eventually the exciton is ionized. This screening also suppresses the Coulomb enhancement factor of the continuum states. The Coulomb screening effect causes a reduction of absorption coefficient near and above band-edge and a bleaching of excitonic resonance [Haug and Schmitt-Rink (1985), Banyai and Koch (1986)]. These nonlinear mechanisms are summarized in Fig. 2 [Gibbons (1987)].

### **Excitonic Optical Nonlinearities in MQW Structures**

A MQW structure consists of alternating ultrathin layer of semiconductors of two different compositions. The band-gaps of these two alternating layers are determined by the semiconductor compositions. Typically, each period of the MQW contains a low band-gap layer sandwiched between two high band-gap layers. In the direction normal to the layers, electrons and holes are confined in the low-gap layer because the neighboring layers have high potentials. In contrast, along the plane of layers, the electrons and holes can move freely. Since the electrons and holes in a MQW can only move freely in two dimensions (2-D), the optical properties of the MQWs are different from those of the three dimensional (3-D) bulk materials.

A schematic representation of a MQW is shown in Fig. 3 [Chavez-Pirson (1989)].

To calculate the linear absorption spectra of the MQWs near the band-edge, the quasi-two dimensional Coulomb interaction must be taken into account. The calculated absorption spectrum of a 2-D MQW shows several important differences from that of bulk. First, the density of states in 2-D is step-like, while in 3-D it is proportional to  $\sqrt{\hbar\omega - E_g}$ . The binding energy of a exciton in 2-D is

$$E_n = \frac{E_R}{(n+1/2)^2}, \quad (1)$$

where  $n$  is the principal quantum number, and  $E_R$  is the exciton Rydberg energy. The binding energy of a exciton in 3-D is

$$E_n = \frac{E_R}{n^2}. \quad (2)$$

The 2-D exciton has larger binding energy than the 3-D. The binding energy of the first (1s) exciton state in 2-D is four times that of the first exciton state in 3-D. The 2-D Bohr radius is half of the 3-D value. In 3-D, the exciton binding energy, through its dependence on dielectric constant and effective masses, scales roughly as the band-gap. The dominating exciton-phonon interaction in semiconductors is due to LO phonons and this interaction strength, through the dependence on the ionicity, also scales approximately as the band-gap. So, in 3-D semiconductors, increasing the exciton binding energy also increases sensitivity to thermal broadening and exciton resonances are only seen at low temperatures almost regardless of band gap energy [Haug (1988)]. In MQWs, the increased binding energy is a result of the artificial reduction of the electron-hole separation by the confinement effect, without any significant change of the coupling to LO phonons [Haug (1988)]. The 2-D 1s-exciton absorption peak is better resolved spectrally than the 3-D as a result of its four times large binding energy.

The dominant nonlinear optical mechanisms in MQWs are different from those in bulk semiconductors. It is important to note the Coulomb screening in MQWs is reduced in

comparison with the 3-D bulk semiconductors [Schmitt-Rink (1985)]. The main contributions to the optical nonlinearities in 2-D are phase space filling and exchange effects [Schmitt-Rink (1985), Haug (1988)]. The exchange effect in 2-D is same as in bulk. As the carrier density increases, the carriers are forced closer together. The exchange interactions between identical particles reduce the spatial correlation and therefore decrease the single particle energy and shrink the band-gap. The phase space filling effect happens as the states in phase space that are already occupied are no longer accessible in optical transitions or available for exciton formation. Both phase space filling and exchange effects are efficient at short distances, so the influences of these two effects in 2-D, where particles see more of their neighbors than in 3-D, are larger than in 3-D. As the carrier density increases, the exciton resonances become bleached because of the phase space filling and exchange effects.

#### Room-Temperature Optical Nonlinearities of GaInAs/AlInAs and GaAlInAs/alInAs Multiple Quantum Wells at 1.3 $\mu\text{m}$

Previous studies have been made of optical nonlinearities in both GaInAs/AlInAs [Weiner *et al.* (1986)] and GaInAs/InP [Fox *et al.* (1987), Fisher (1990)] MQWs near 1.5  $\mu\text{m}$ . Transient nonlinear absorption spectra of GaInAs/AlInAs near 1.3  $\mu\text{m}$  at 10 K have been reported [Elsaesse *et al.* (1989), Lobentanzer (1989)]. An optical logic etalon of an GaInAs/InP MQW at 1.55  $\mu\text{m}$  operating at 77 K has also been demonstrated with a 20:1 contrast and nanosecond recovery time [Tai *et al.* (1987)]. A room-temperature optically bistable device in a GaInAs/AlInAs MQW etalon at 1.5  $\mu\text{m}$  was also demonstrated [Kawaguchi *et al.* (1987)]. However, there has been no report to date on the room-temperature nonlinear optical properties of GaInAs/AlInAs and GaAlInAs/AlInAs MQWs and the performance of optical logic devices made from these materials at 1.3  $\mu\text{m}$ . In this section we report room-temperature measurements of the nonlinear absorption spectra, saturation carrier densities and carrier recovery times for both a 40 Å GaInAs/AlInAs and a 90 Å GaAlInAs/AlInAs MQW sample.

The nonlinear absorption spectra and saturation carrier densities of MBE grown  $\text{Ga}_{0.376}\text{Al}_{0.094}\text{In}_{0.53}\text{As}/\text{Al}_{0.48}\text{In}_{0.52}\text{As}$  and  $\text{Ga}_{0.47}\text{In}_{0.53}\text{As}/\text{Al}_{0.48}\text{In}_{0.52}\text{As}$  MQW structures were measured in this experiment. The detailed growth conditions of the samples were previously described [Khitrova *et al.* (1990)]. The GaInAs/AlInAs MQW consists of 100 periods of 40 Å GaInAs wells and 68 Å AlInAs barriers. The quaternary GaAlInAs/AlInAs MQW sample has 100 periods of 90 Å GaAlInAs wells and 69 Å AlInAs barriers. Both MQWs have heavy-hole exciton peaks near 1.3 μm at room temperature. In the ternary system, the transition energy of the exciton can be adjusted by changing the quantum well thickness. For the quaternary system, both the well thickness and the Ga/Al ratio can be used to shift the exciton absorption peak. The latter affords the opportunity to tailor other parameters such as the carrier lifetime or exciton sharpness while maintaining the exciton at the same wavelength [Khitrova *et al.* (1990)].

The absorption spectra of both samples were examined in a pump-probe geometry shown as Fig. 4. The 1.064 μm line from a Q-switched Nd:YAG laser with a 10 Hz repetition rate was used for the pump beam. The pump beam frequency was enough above the absorption band-edge of all samples to efficiently generate electron and hole pairs. The probe beam was generated by difference frequency mixing of the 1.064 μm line of a YAG laser and the output of a tunable Rhodamine 6G dye laser in a  $\text{LiIO}_3$  crystal. The tunable range of the infrared beam, from 1220 nm to 1350 nm, covered the band-edge region of all samples. The pump pulse and probe pulse were 10 ns and 4 ns in duration, respectively. The samples were mounted on a rotation stage which was adjusted to Brewster's angle to minimize Fabry-Perot oscillations in the absorption spectra. The pump and probe beams were overlapped on the sample in both space and time with spot diameters of 135 μm and 37 μm, respectively. The large pump beam eliminated diffusion of the carriers from the probed region. The polarization of the pump beam was orthogonal to that of the probe beam so that an analyzer could selectively block the pump beam. The probe beam was divided with one beam focused on a Ge detector as the reference signal and the other beam focused on the sample, then imaged onto another Ge detector which measured the transmitted signal. The reference and transmitted signals were averaged over 100 laser shots by a boxcar integrator. The relative transmission values for the samples were obtained

from the ratios between the transmitted and the reference signals. The absolute transmission value for the samples was obtained from the ratio of the relative transmission with and without the sample.

The nonlinear absorption spectra measured at room temperature with pump intensities of 0, 1.6, 3.1, and 17.0 kW/cm<sup>2</sup> on the 40 Å GaInAs/AlInAs MQW are shown in Fig. 5 (a). The latter three pump beam intensities correspond to photo-generated carrier densities of  $6.4 \times 10^{17}$ ,  $1.2 \times 10^{18}$ , and  $6.7 \times 10^{18}$  cm<sup>-3</sup> and are calculated from the well known rate equation,

$$\frac{dN}{dt} = \frac{\alpha I}{\hbar \omega} - \frac{N}{\tau}, \quad (3)$$

where  $\tau$  is the lifetime of the electron-hole pairs,  $\omega$  is the pump beam frequency,  $I$  is the pump beam intensity, and  $\alpha$  is the absorption coefficient at the pump beam frequency. Using a Gaussian temporal profile for the pump beam, the solution of equation (3) is the following:

$$N(t) = \frac{e^{-t/\tau} \alpha I_0}{\hbar \omega} \times \int_{-x}^t e^{-t'/\tau} \exp \left[ - \left( \frac{1.6651 t'}{\text{FWHM}} \right)^2 \right] dt', \quad (4)$$

where  $I_0$  is the peak pump beam intensity, FWHM is pulse width at half-maximum of the pump beam,  $x$  is twice FWHM, and  $t$  is the delay time between the pump and probe, which is 0 ns in this experiment. For this calculation, we used our measured electron-hole pair lifetime values  $\tau$  and the reflection loss of the pump beam at the sample surface was taken into account.

In the linear absorption spectrum of the 40 Å MQW, we observed well-resolved heavy-hole and light-hole excitonic resonances located at 1315 nm and 1225 nm, respectively. The half-width of the lowest exciton peak is about 14 meV [Khitrova *et al.* (1990)]. As shown in Fig. 5 (a), the exciton resonances bleach and broaden with increasing pump beam intensities. Phase-space filling and exchange effects are believed to be the dominant nonlinear mechanisms for saturation of the excitons in MQWs [Schmitt-Rink *et al.* (1985), Weiner *et al.* (1986), Haug (1988)]. Note that the influence of Coulomb screening in quasi two-dimensional MQWs is

relatively weak in comparison to the three-dimensional case [Schmitt-Rink *et al.* (1985), Weiner *et al.* (1986), Haug (1988)].

Because the change in absorption at the exciton peak depends on the pump beam intensity only through the photo-generated carriers, we computed the saturation carrier densities for these samples instead of the saturation intensities. The saturation carrier density at the heavy-hole exciton peak was determined by the best fit of the experimental data to the following Lorentzian equation:

$$\alpha L(N) = \alpha_b L + \frac{\alpha_0 L}{1 + N/N_s}, \quad (5)$$

where  $\alpha_0$  and  $\alpha_b$  are the linear and background absorption coefficients at the heavy-hole exciton peak, respectively,  $L$  is the well thickness of the MQW, and  $N_s$  is the saturation carrier density. As shown in Fig. 6 (a), the optical absorption decreases as the carrier density increases. The solid curve is a best fit to the experimental data. The saturation carrier density, linear absorption ( $\alpha_0 L$ ), and background absorption ( $\alpha_b L$ ) were found to be  $1.2 \times 10^{18} \text{ cm}^{-3}$ , 0.88, and 0.88, respectively. The computed saturation carrier density for the GaInAs/AlInAs MQW is close to the reported values for GaAs/AlGaAs MQWs [Park *et al.* (1988)].

Figure 5 (b) shows the room-temperature nonlinear absorption spectra of the GaAlInAs/AlInAs MQW sample for pump beam intensities of 0, 1.7, 5.0, and 21.2 kW/cm<sup>2</sup>. These pump beam intensities generated carrier densities of  $2.1 \times 10^{17}$ ,  $6.2 \times 10^{17}$ , and  $2.6 \times 10^{18} \text{ cm}^{-3}$ , respectively. Note that in Fig. 5 (a) and (b), the residual background absorption of  $\alpha l \approx 0.8$  and 0.4, respectively, at energies below the exciton originates from the reflection and scattering from the sample surfaces. The linear absorption spectrum of the sample also shows two well resolved exciton peaks. The half-width of the lowest exciton peak is about 12 meV [Khitrova *et al.* (1990)]. The exciton peaks of the quaternary MQW are less pronounced than those of the ternary, presumably because 90 Å wells have less confinement than 40 Å wells [Khitrova *et al.* (1990)]. As in the GaInAs/AlInAs MQW case, the presence of increasing pump beam intensity bleaches exciton peaks of GaAlInAs/AlInAs MQW due to phase-space filling and

exchange effects. The saturation carrier density, linear absorption, and background absorption were determined to be  $1.0 \times 10^{18} \text{ cm}^{-3}$ , 0.84, and 0.43, respectively. The computed saturation carrier density for the GaAlInAs/AlInAs MQW is close to the GaInAs/AlInAs MQW. The dependence of the optical absorption on the carrier density in the 90 Å GaAlInAs/AlInAs MQW is shown in Fig. 6 (b).

Normally, the switching time of a nonlinear switching device is limited by the recovery time of carriers because the recombination time of carriers is longer than the time needed to generate carriers. The carrier recovery dynamics of the samples were measured with a picosecond pump-probe set-up (see Fig. 7) [Johns (1991)]. The experiments were performed with a pulse compressed mode-locked Nd:YAG laser at a 100 MHz repetition rate. Both pump and probe beams had a 2 ps duration at a wavelength of 1319 nm which coincides with the heavy-hole exciton peak. The pump and probe beams were overlapped on the samples with a 26  $\mu\text{m}$  diameter. The pump beam was polarized orthogonally to the probe beam. An analyzer and a aperture were placed in front of the detector to isolate the probe from any scattering from the pump. The time delay between the pump and probe beam was varied from -50 ps to 450 ps. Figure 8 shows the probe transmission as a function of the pump-probe delay for a pumping power of 20 mW on the 90 Å GaAlInAs/AlInAs MQW. This pumping power corresponds to a photo-generated carrier density of  $1.7 \times 10^{18} \text{ cm}^{-3}$ . The exponential fit of the data resulted in a 750 ps lifetime for the 90 Å MQW. The lifetime for the 40 Å ternary MQW is longer, with a value of  $\approx 5.3 \text{ ns}$ . The lifetime for the quaternary MQW is shorter than that for the ternary MQW, probably due to the presence of aluminum in the quaternary MQW, which may affect the carrier lifetime [Khitrova *et al.* (1991a)]. To check the effects of lateral diffusion on the absorption recovery time, the diffusion equation [Kittle (1966)] was used to determine changes in the average carrier density. In this calculation, the ambipolar diffusion constant  $D \approx 15 \text{ cm}^2/\text{s}$  was determined by carrier mobilities of  $10500 \text{ cm}^2/\text{Vs}$  for electrons and  $300 \text{ cm}^2/\text{Vs}$  for holes [Pearsall (1982)]. The diffusion calculation indicates that 500 ps after excitation, the average carrier density decreases less than 1% for a 26  $\mu\text{m}$  diameter spot. Thus, the small lateral diffusion of the carriers does not play an important role in the picosecond recovery of the



absorption changes.

### Nonlinear Fabry-Perot Etalon

A FP etalon consists of two high reflectors or flat mirrors placed in parallel and held a fixed distance apart by a spacer. Because of the high reflectivity of the mirrors, the light undergoes multiple reflections in the mirrors. If the light inside the cavity is sufficiently coherent, the interference will occur between the multiple reflected beams. If the phase shift between the successive beams is an integral multiple of  $2\pi$ , the interference will be constructive. In this case, the transmission through the etalon will be at a maximum and this result is the well-known "standing-wave" resonance condition

$$L = \frac{m\lambda_R}{2n}, \quad (6)$$

where  $L$  is the cavity length,  $m$  is the order number,  $n$  is the refractive index, and  $\lambda_R$  is resonance wavelength in vacuum.

A nonlinear optical FP etalon is a FP interferometer with a material used for the spacer which has an intensity-dependent absorption and index of refraction. To qualitatively understand the operation of the nonlinear optical Fabry-Perot etalon, a medium with negative nonlinear refractive index is considered. As the index of refraction decreases, which results from the presence of the pump beam on the nonlinear etalon, the resonance wavelength must also decrease; ie., the transmission peak shifts to a shorter wavelength. Therefore, for a probe wavelength  $\lambda < \lambda_R$ , when the pump beam intensity increases, the probe transmission at  $\lambda$  increases. By continuing to increase the pump beam intensity, the probe transmission will become resonant. In this case, the probe transmission is switched from the "off resonance" state to the "on resonance" state by increasing the pump beam intensity. On the contrary, if the the probe beam wavelength is originally on the transmission peak, the presence of the pump beam will switch the probe transmission from the "on resonance" state to the "off resonance" state.

In general, the nonlinear FP etalon can be operated by the pump-probe technique. The pump beam is used for changing the refractive index of the spacer, so it is necessary to tune the pump beam above the absorption band-edge of the spacer. Since the probe beam is used to probe the transmission of the cavity, it is desirable to set the probe beam below the absorption band-edge of the spacer [Jewell *et al.* (1984, 1985, and 1987)]. Typically, the front mirror is highly transmitting and rear mirror is highly reflecting for the pump beam. For the probe beam, both mirrors are highly reflecting to optimize the cavity finesse.

### Design and Fabrication

Two categories of high reflectors are used in the nonlinear optical FP etalon. The first uses high reflection dielectric thin film multilayer structures for the reflectors. These high reflection multilayer structures are attached or coated on the epitaxially grown semiconductor materials to form a cavity for photonic switching [Gourley *et al.* (1986), Jewell *et al.* (1987), Tai *et al.* (1987), Kawaguchi *et al.* (1987), Sfez *et al.* (1990), Kuszelewicz *et al.* (1990)]. However this type of etalon is highly nonuniform, either due to wedges produced in the semiconductor material as a result of the etching process or due to the nonparallel alignment of the reflectors [Chavez-Pirson (1989)]. The other FP structure, which is called an integrated mirror etalon, is grown monolithically for the whole etalon by using well-developed crystal grown technology such as MBE. The high reflector used in this integrated FP etalon structure is a quarterwave stack, consisting of alternating layers of high and low index semiconductors with the optical thickness of each layer equal to a quarter of the design wavelength, i.e.,

$$n_h d_h = n_l d_l = \frac{\lambda}{4}. \quad (7)$$

The detailed design of a nonlinear integrated mirror etalon has been previously described [Chavez-Pirson (1989), Chuang (1991)]. The design of the etalon first must consider the operating wavelength, the reflectivity, spectral bandwidth, and the center wavelength of

reflectors. Then the thickness of each layer for both the high reflectors and spacer, the number of layers, the types of materials for both high reflectors and spacer regions, and the structure of the spacer region must be considered. In general, the design of the integrated mirror etalon can be approached as follows: the operating wavelength of the switching etalon need to be determined, and this parameter will determine what substrate should be used for the MBE growth. For example, if the wavelength is chosen in the 0.8  $\mu\text{m}$  to 1.1  $\mu\text{m}$  region, a GaAs substrate should be used; on the other hand, if the wavelength is around 1.3  $\mu\text{m}$  or 1.5  $\mu\text{m}$ , an InP substrate must be used. The lattice-matching requirement in the epitaxial grown monolithic structure then limits the choice of materials for the reflectors and spacer. Next the thickness of the high and low refractive index layers of high reflectors must be calculated using the refractive index values at the operating wavelength. The numbers of layers in the reflectors are then determined according to the specified reflectance of the reflectors or the finesse of the cavity. The material and structure of the spacer region is determined by the operating wavelength as well as the specific properties desired. The spacer layer must be chosen properly so that the resonance wavelength of the etalon has the proper detuning from the optical absorption band-edge to yield a high finesse cavity with enough nonlinear index change to produce optical switching. The electric field distribution of the whole structure must be calculated to ensure the position of the active spacer layer. Note that the effective cavity length, defined by the length where light will bounce back and forth, is longer than the physical spacer length since the electric field extends into the quarterwave stacks [Jewell *et al.* (1988), Chuang (1991)]. This means the equation usually used for calculating the spacing of transmission peaks in FP transmission spectrum shown as below is no longer true

$$\Delta\lambda = \frac{\lambda^2}{2nL}, \quad (8)$$

where  $L$  is the length of the spacer layer. A schematic structure of an optical integrated mirror etalon is shown as Fig. 9.

The MBE-grown integrated mirror etalons at 1.3  $\mu\text{m}$  were designed and fabricated by Khitrova *et al.* [Khitrova *et al.* (1991b)] as the photonic switching devices for optical fiber communication systems. The etalons were designed for the control beam at a shorter wavelength ( $\approx 1.25 \mu\text{m}$ ) for efficient generation of carriers and the probe beam at a longer wavelength ( $\approx 1.30 \mu\text{m}$ ) for low absorption and high Fabry-Perot finesse. The challenge is to grow MQW material between very thick ( $> 20$  quarterwave layers on each side) integrated mirrors, lattice-matched to the InP substrate and with a band-edge close to but shorter in wavelength than 1.3  $\mu\text{m}$  [Khitrova *et al.* (1991b)].

The high reflectors are formed by alternately growing quarterwave layers of high (GaAlInAs) and low (AlInAs) index. The absorption band-edge of GaAlInAs can be controlled by the ratio of Ga:Al and this ratio was set at a small value so that the reflectors have no absorption at the operating wavelength. The refractive index difference between these materials is  $\approx 0.25$  although this varies with wavelength. Compared with the larger index difference ( $\approx 0.7$ ) for AlGaAs/AlAs [Chavez-Pirson (1989), Chuang (1991)], the small difference of index refraction means the reflectors require a larger number of quarterwave layers to have the same reflectivity. The mirrors in the etalons consist of 12 periods of 91.4 nm of  $\text{Ga}_{0.33}\text{Al}_{0.15}\text{In}_{0.52}\text{As}$  and 99.0 nm of  $\text{Al}_{0.48}\text{In}_{0.52}\text{As}$ . The mirrors have reflectivities higher than 0.7 from 1278 to 1361 nm.

The nonlinear spacer layer consists of GaInAs/AlInAs MQWs with exciton features near 1.3  $\mu\text{m}$  [Khitrova *et al.* (1990), Hsu *et al.* (1991)]. The band-edge of the MQWs can be controlled by the the well width and the band-edge is reasonably sharp so that large nonlinear index exists simultaneously with low absorption at the probe wavelength. The spacer has 108  $\text{Ga}_{0.47}\text{In}_{0.53}\text{As}/\text{Al}_{0.48}\text{In}_{0.52}\text{As}$  MQWs with 35 Å wells and 58 Å barriers and band-edge at 1.25  $\mu\text{m}$ .

The transmission spectra taken at two different positions of a integrated mirror etalon, shown in Fig. 10 (a) and (b) [Khitrova *et al.* (1991b)], show the etalon peaks located at different wavelengths for these two positions and this is mainly due to the thickness variation in the etalon. As shown in Fig 10 (a), the two etalon peaks are at 1250 and 1320 nm, but in Fig. 10 (b), the two etalon transmission resonance are shifted to 1280 and 1350 nm, respectively.

Because the two etalon fringes in Fig. 10 (b) have a larger detuning relative to the absorption band-edge of the spacer than those of in Fig. 10 (a), the FP transmission peaks in Fig. 10 (b) have larger values. The transmission fringe, at shorter wavelengths shown in both Fig. 10 (a) and (b) have small finesse and this is a result of low reflectivity of mirrors and absorption by the spacer in this wavelength region.

### **The Recovery Time Measurements of Integrated Mirror Etalons at 1.3 $\mu\text{m}$**

The switching recovery times of two integrated mirror etalons were investigated by the previously described pump-probe set up with a 2 ps duration at 1319 nm (see Fig. 7). No change in transmission was observed for the FP etalon which was designed for the control beam at 1.25  $\mu\text{m}$  and the probe beam at 1.3  $\mu\text{m}$  (the transmission spectrum is shown in Fig. 10). The pump beam wavelength 1.319  $\mu\text{m}$  is below the band-edge of the spacer (1.25  $\mu\text{m}$ ) so that few carriers are generated and this might be the reason for a lack of change in the transmission in this etalon. Another GaInAs FP etalon was used to measure the recovery time of the device. The absorption band-edge of the spacer is near 1.32  $\mu\text{m}$  and the high absorption effect from the spacer reduces the transmission peaks of this etalon. Only 20% transmission was observed at the peaks. The transmission spectrum of this etalon is shown in Fig. 11 (a). The pump beam at 1.319  $\mu\text{m}$  was efficient enough to generate nonlinearities, in the spacer so that a change of transmission was observed in this case. As shown in Fig. 11 (b), the GaInAs/AlInAs FP etalon has a 125 ps recovery time, with a fast switch-on speed. Due to the limited translation from the positioning equipment available, we could not measure the delay beyond 500 ps. It is probable that the transmission drops below the baseline as a result of heating of the sample (which shifts the transmission fringe to a longer wavelength) by the high repetition rate pulser laser in our experiment. The faster recovery of the etalon compared with the MQWs may be associated with poorer quality MQWs in the etalon grown on top of 12 pairs of quarter-wave layers.

## Conclusions

In conclusion, the nonlinear optical properties of both bulk and MQWs semiconductor materials are reviewed. We have measured optical nonlinearities and recovery time of carriers at 1.3  $\mu\text{m}$  for two MQW structures of epitaxially-grown GaAlInAs/AlInAs and GaInAs/AlInAs at room temperature. Saturation carrier densities at the heavy-hole exciton peak were determined to be  $1.2 \times 10^{18}$  and  $1.0 \times 10^{18} \text{ cm}^{-3}$  with carrier recovery times of  $\approx 5 \text{ ns}$  and  $\approx 750 \text{ ps}$  for GaInAs/AlInAs and GaAlInAs/AlInAs MQWs, respectively. These measured carrier density are close to the reported values for GaAs/AlInAs MQWs. Nonlinear integrated FP etalon logic gates were designed and fabricated for a high-speed optical switching device with a recovery time of 125 ps near 1.3  $\mu\text{m}$  operated at room temperature. These devices are potentially useful for development of a multi-giga-bit optical time-division demultiplexed interconnection system at 1.3  $\mu\text{m}$  where ultrafast optical processing elements are needed.

## Future Work

For future studies of this work, two types of all-optical devices are probably the direction for the development of high-contrast fast-speed switching elements at 1.3  $\mu\text{m}$ . The first device is a asymmetric etalon made from GaInAs/AlInAs or GaAlInAs/AlInAs MQWs. It has been reported that a GaAs/AlGaAs all-optical asymmetric reflection modulator can be switched at 2.5 mW with a 27:1 contrast ratio [Heffernan *et al.* (1991)]. Asymmetric reflection modulators based on GaInAs or GaAlInAs material would be one of the approaches to obtain high contrast all-optical switching elements at 1.3  $\mu\text{m}$ .

The second device is the switching element that is based on a GaInAs/AlInAs or GaAlInAs/AlInAs tunneling biquantum well structure (BQW). It was reported that a GaAs/AlGaAs BQW exhibits picosecond recovery of excitonic absorption near 0.85  $\mu\text{m}$  [Tackeuchi *et al* (1991)]. A FP etalon device utilizing the GaInAs or GaAlInAs BQW structure would be one of the approaches to be considered for high speed all-optical switching elements at 1.3  $\mu\text{m}$ .

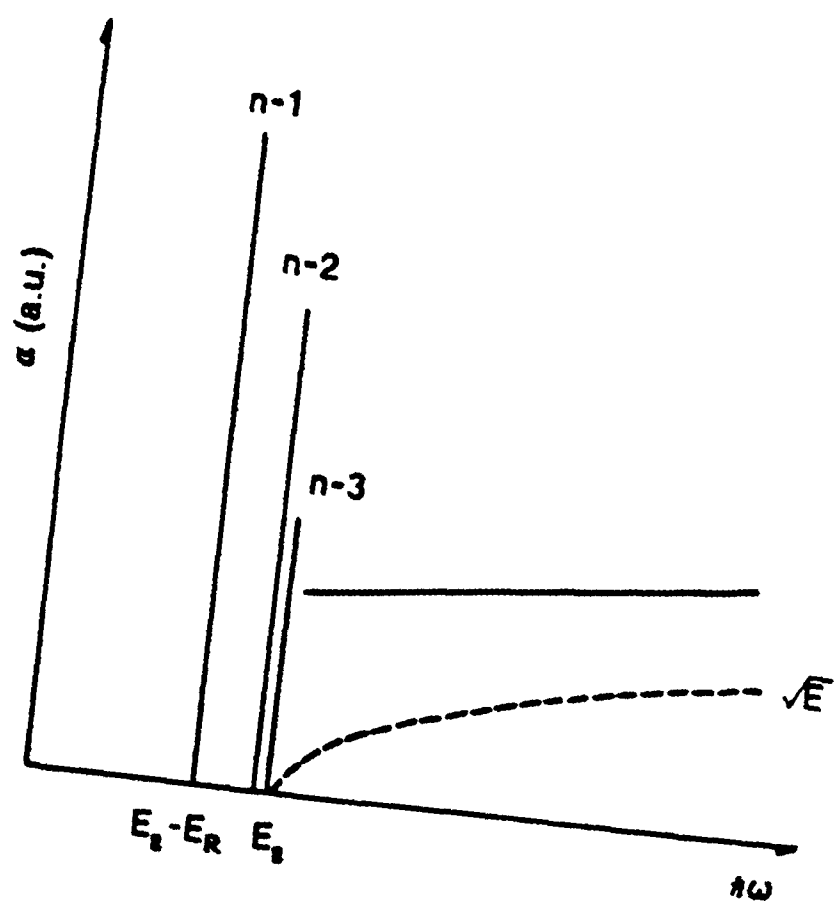


Fig. 1 Schematic diagram of the absorption spectrum with inclusion of Coulomb interaction. The dashed line is the absorption spectrum without considering Coulomb interaction [Bassani (1975)].

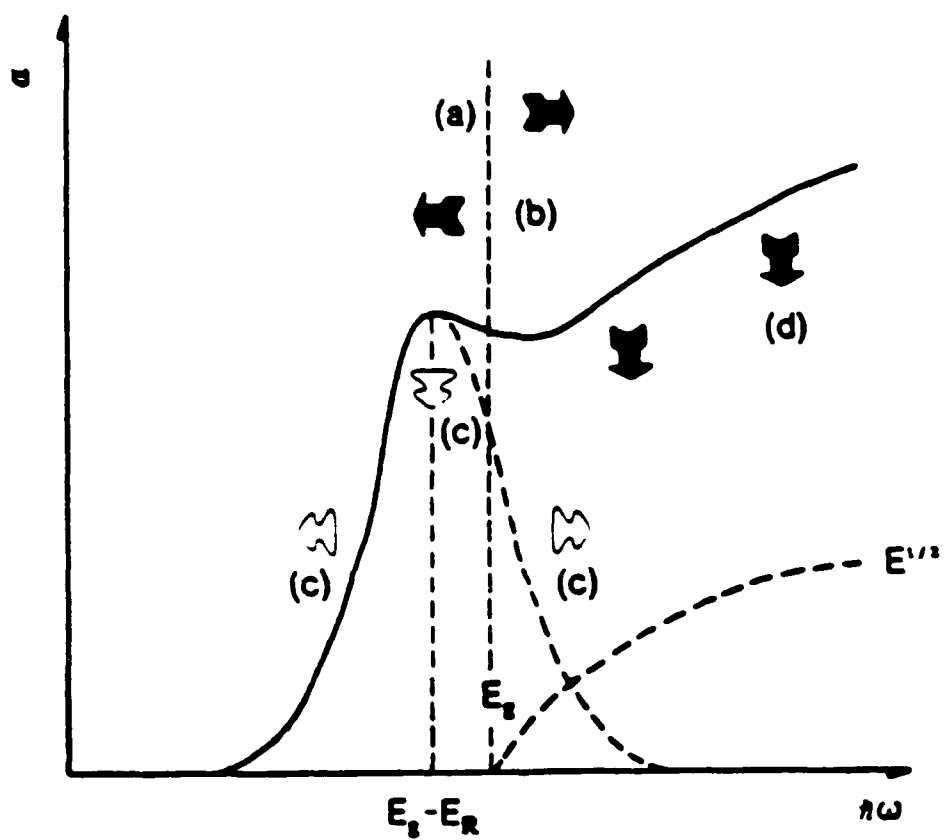


Fig. 2 Nonlinear optical absorption spectra of a direct-gap semiconductor. (a) band filling effect shifts the band-edge to higher energy side; (b) bandgap renormalization shifts the band-edge to lower energy side; (c) screening effect broadens and saturates excitons; (d) reduction of the Coulomb enhanced states [Gibbons (1988)].



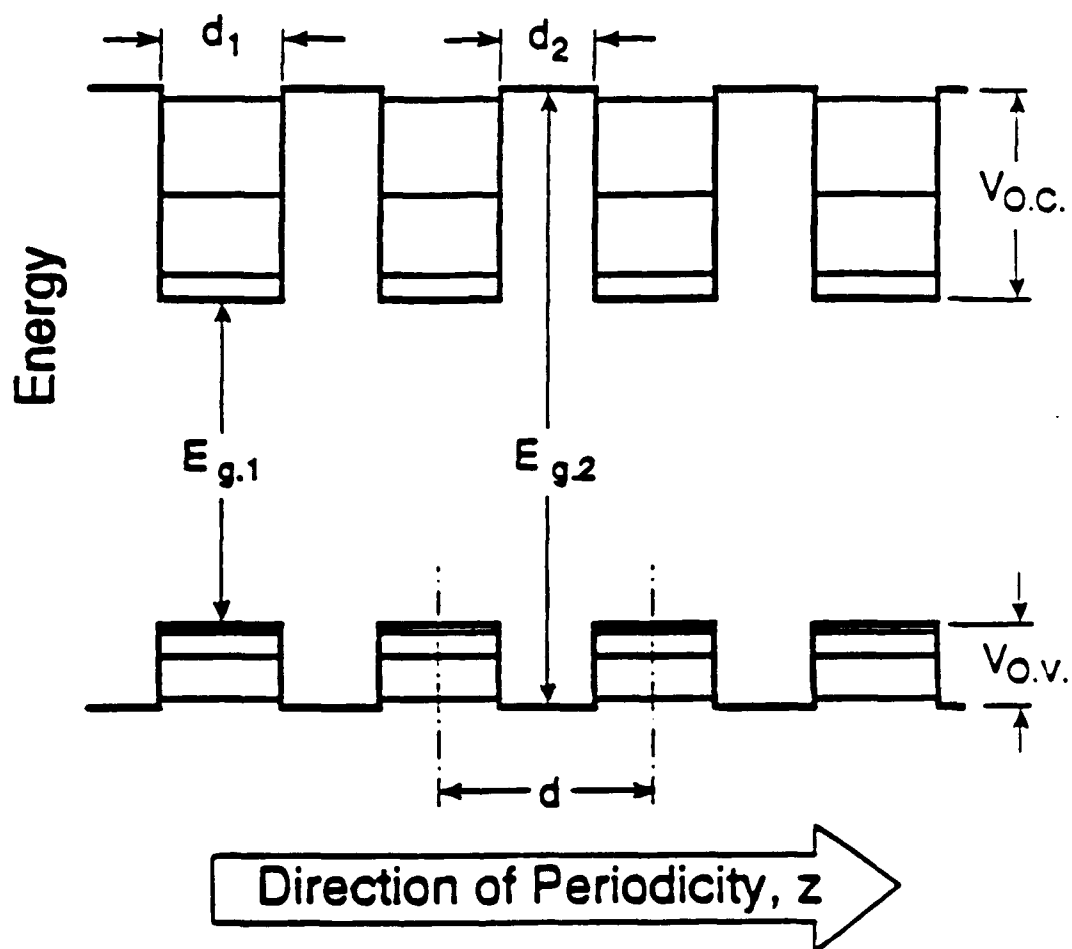


Fig. 3 Schematic representation of a multiple-quantum-well structure [Chavez-Pirson (1989)].



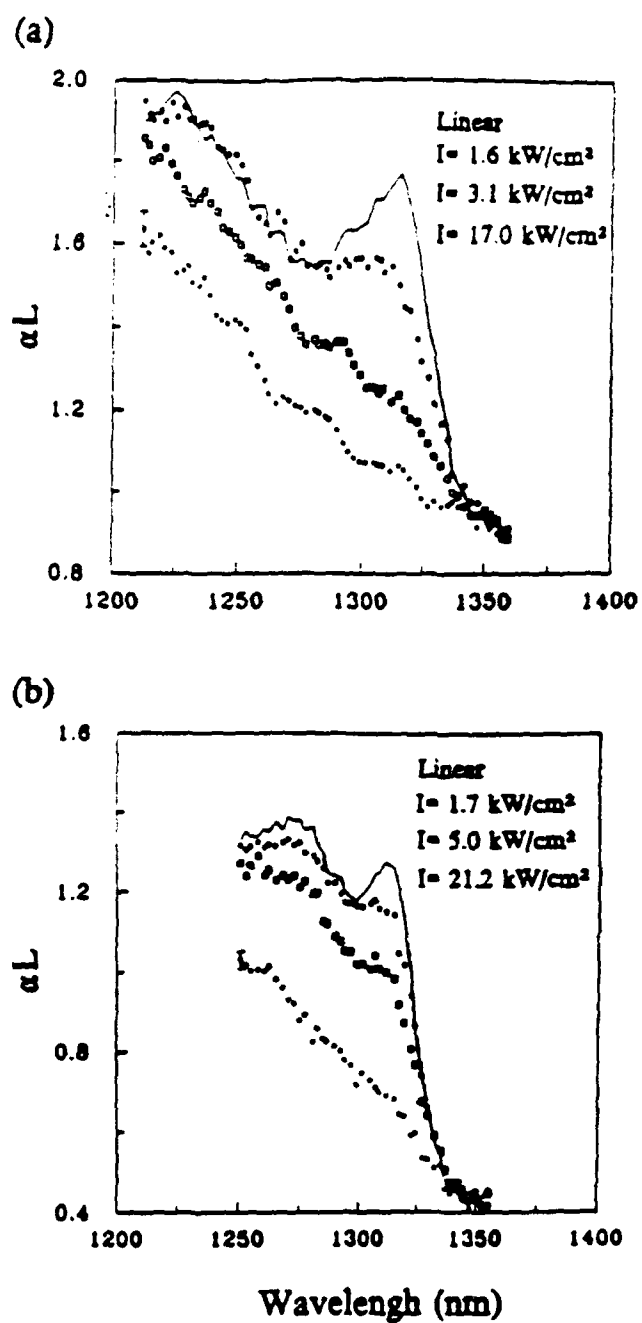


Fig. 5 (a) The absorption spectra of the 40 Å GaInAs/AlInAs MQW for various pump beam intensities. (b) The absorption spectra of the 90 Å GaInAs/AlInAs MQW for various pump beam intensities.

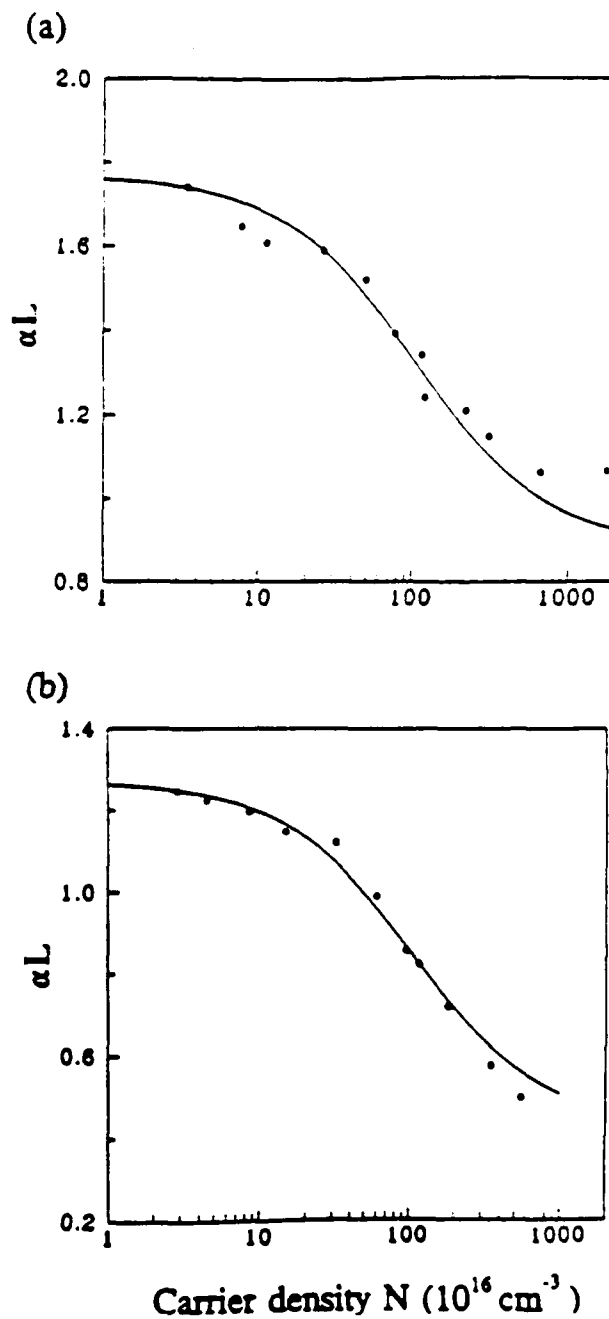


Fig. 6 (a) Optical absorption dependence of carriers density in the 40 Å GaInAs/AlInAs MQW. The black points are experimental data and the solid curve is the best fit of the experimental data. (b) same as (a) but for the 90 Å GaAlInAs/AlInAs MQW.

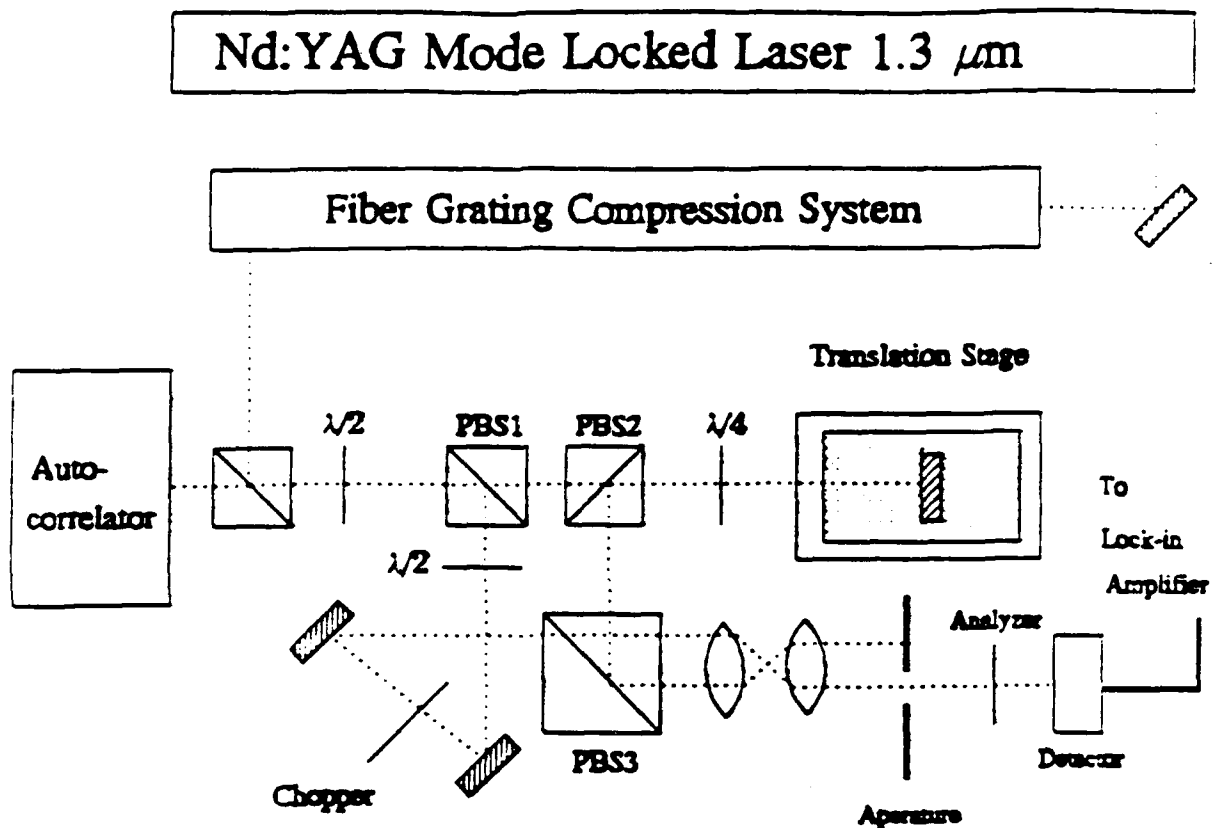


Fig. 7 Picosecond pump-probe experiment set-up for measuring the recovery time of MQWs and integrated mirror etalons [Johns (1991)].

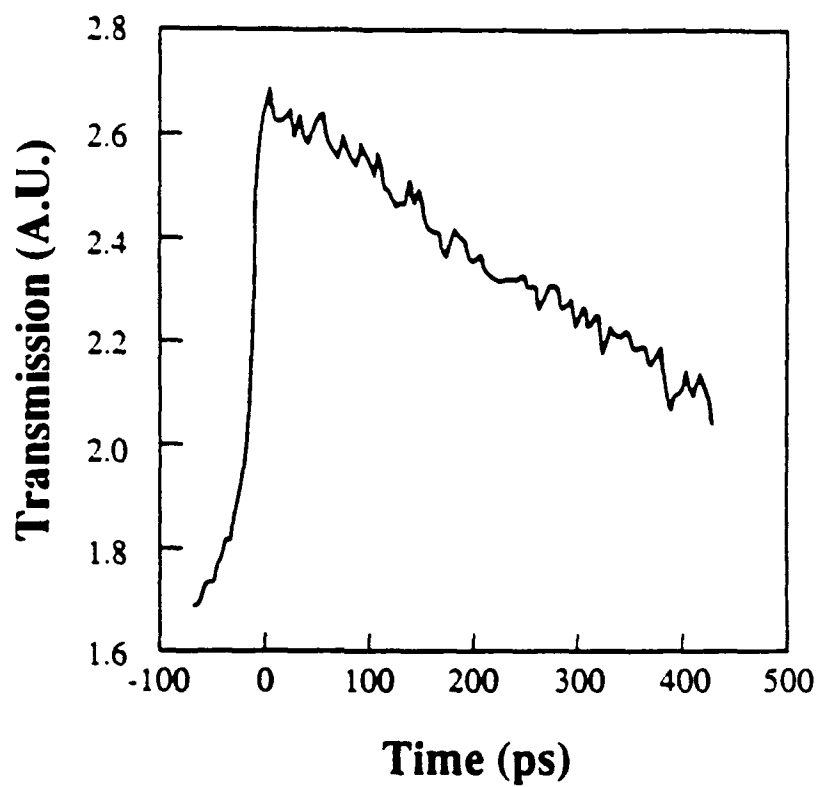


Fig. 8 The probe transmission as a function of the pump-probe time delay for the 90 Å GaAlInAs/AlInAs MQW.

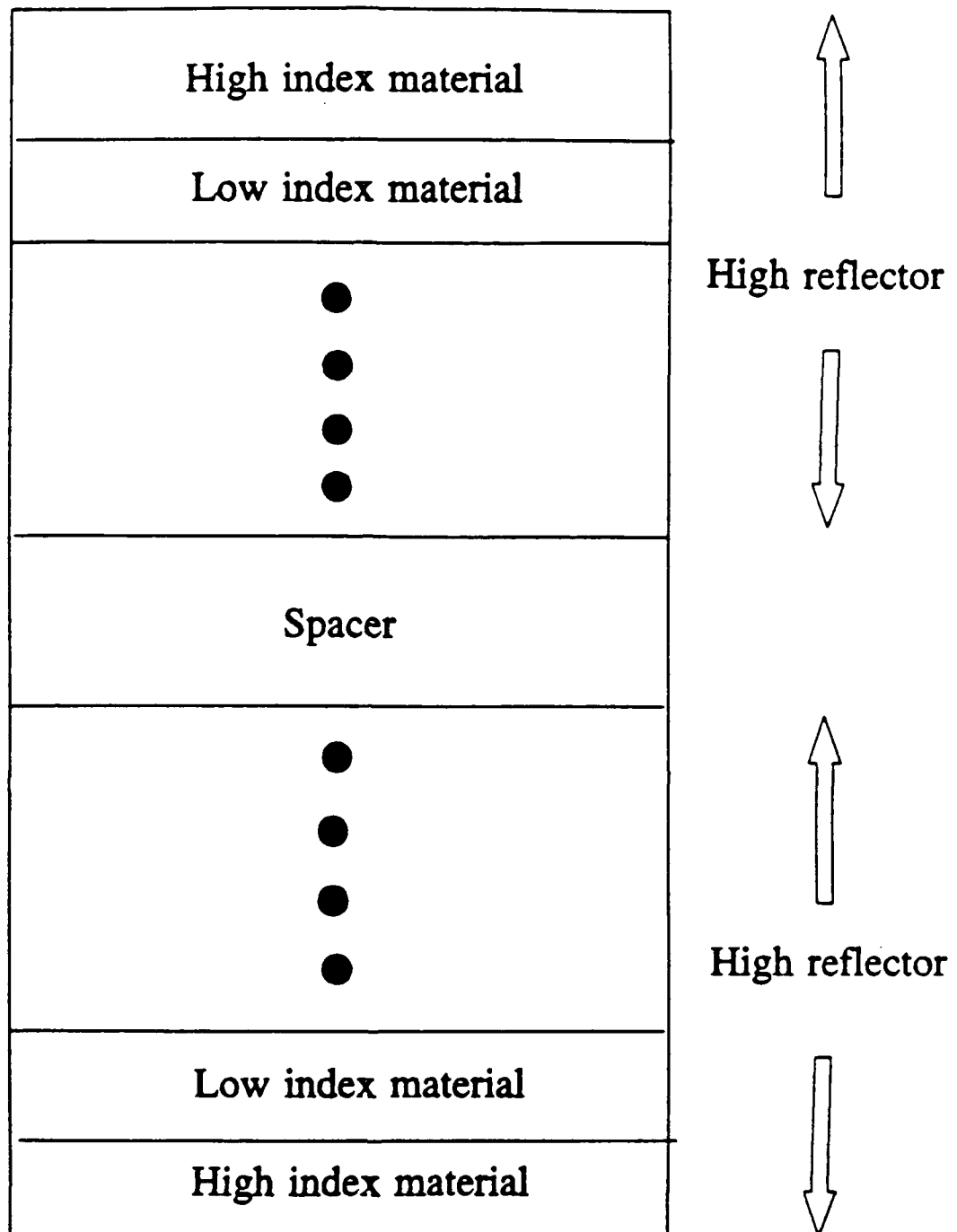


Fig. 9 Schematic diagram of an integrated mirror etalon.

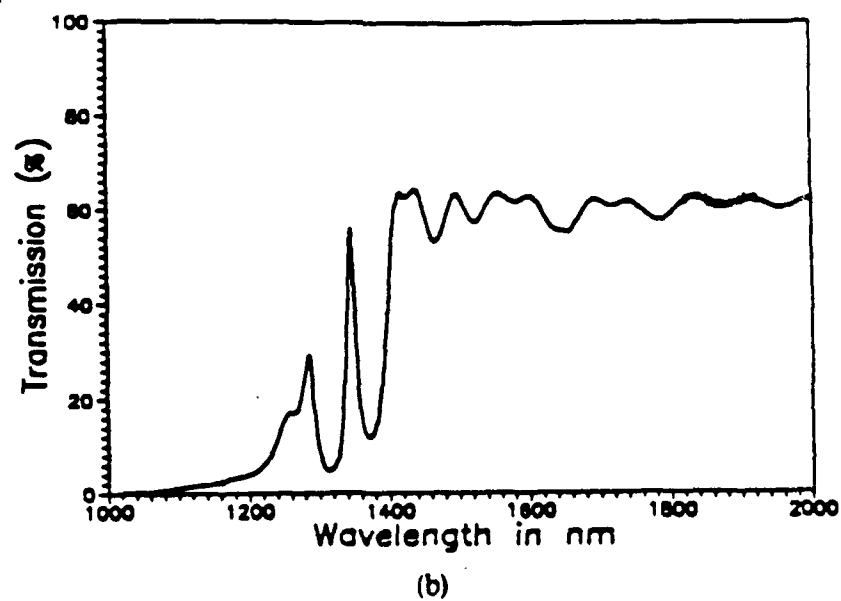
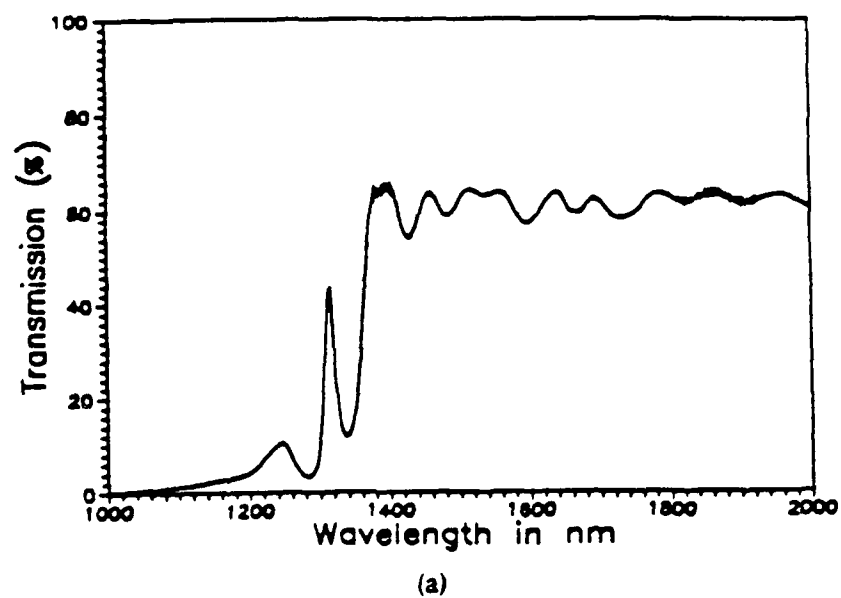


Fig. 10 (a) and (b) are linear transmission spectra on two different positions on the integrated mirror etalon [Khitrova et. al. (1991)].



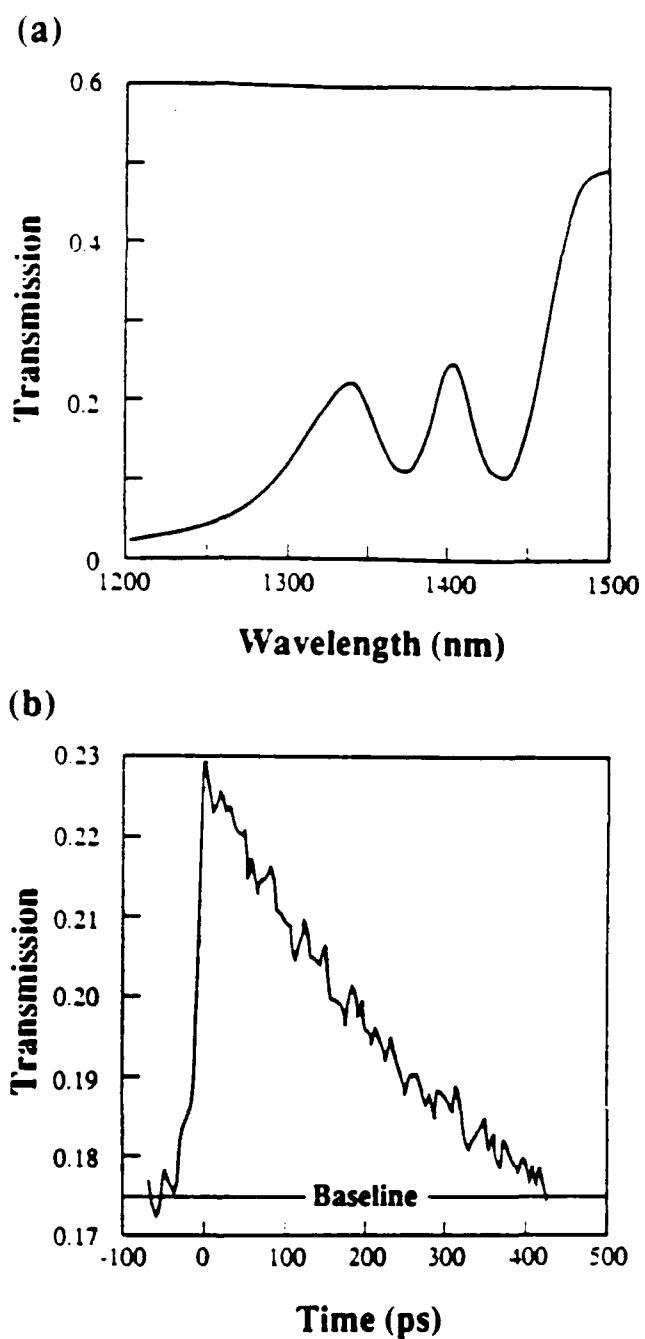


Fig. 11 (a) The linear transmission fringe of a GaInAs/AlInAs integrated mirror etalon. (b) Measured switching time of the room-temperature of the optical logic gate of Fig. 4-11 (a).

## References

- Banyai, L., and Koch, S. W., *Z. Phys. B* **63**, 283 (1986).
- Bassani, F., *Electronic States and Optical Transitions in Solids* (Pergmon, Oxford, 1975).
- Chavez-Pirson, A., Ph.D. dissertation, University of Arizona, Tucson (1989).
- Chemla, D. S., Miller, D. A. B., Smith, P. W., Gossard, A. C., and Wiegmann, W., *IEEE J. Quantum Electron.* **20**, 265 (1984).
- Chemla, D. S. and Miller, D. A. B., *J. Opt. Soc. Am. B*, **2**, 1155 (1985).
- Cho, K., *Excitons* (Springer-Verlag, Berlin, 1979).
- Chuang, C. L., Ph.D. dissertation, University of Arizona, Tucson (1991).
- Elliot, R. J., *Phys. Rev.* **108**, 1384 (1957).
- Elsaesser, T., Bauerle, R. J., Kaiser, W., Lobentanzer, H., Stolz, W., and Ploog, K., *Appl. Phys. Lett.* **54**, 256 (1989).
- Fisher, M. A., *J. Appl. Phys.* **67**, 543 (1990).
- Fox, A. M., Maciel, A. C., Schorthose, M. G., Ryan, J. F., Scott, M. D., Avies, J. I., and Riffat, J. R., *Appl. Phys. Lett.* **51**, 30 (1987).
- Friberg, S. R., Silberberg, Y., Oliver, M. K., Andrejco, M. J., Saifi, M. A., and Smith, P. W., *Appl Phys Lett.* **51**, 1135 (1987).
- Gibbs, H. M., Khitrova, G., and Peyghambarian, N. eds., *Nonlinear Photonics* (Springer, Berlin, 1990).
- Gibbons, W. M., Ph.D. dissertation University of Arizona, Tucson (1987).
- Gourley, P. L. and Drummond, T. J., *Appl. Phys. Lett.* **49**, 489 (1986).
- Haug, H., ed., *Optical Nonlinearities and Instabilities of Semiconductors* (Academic Press, New York, 1988).
- Haug, H. and Schmitt-Rink, S., *J. Opt. Soc. Am. B*, **2**, 1135 (1985).
- Heffernan, J. F., Moloney, M. H., Hegarty, J., Roberts, J. S., and Whitehead, M., WE8-1, OSA Photon. Switch. Top. Meet. Salt Lake City, UT (1991).
- Hsu, C. C., McGinnis, B. P., Sokoloff, J. P., Khitrova, G., Gibbs, H. M., Peyghambarian, N., Johns, S. T., and Krol, M. F., submitted to *J. Appl. Phys.* (1991).
- Hulin, D., Mysyrowicz, A., Antonetti, A., Migus, A., Masselink, W. T., Markoc, H., Gibbs, H. M., and Peyghambarian, N., *Appl. Phys. Lett.* **49**, 749 (1986).
- Jewell, J. L., Rushford, M. C., and Gibbs, H. M., *Appl. Phys. Lett.* **44**, 172 (1984).
- Jewell, J. L., Lee, Y. H., Warren, M., Gibbs, H. M., Peyghambarian, N., Gossard, A. C., and Wiegman, W., *Appl. Phys. Lett.* **46**, 918 (1985).
- Jewell, J. L., Scherer, A., McCall, S. L., Gossard, A. C., and English, J. H., *Appl. Phys. Lett.* **51**, 94 (1987).

- Jewell, J. L., Lee, Y. H., McCall, S. L., Harbison, J. P., and Florez, L. T., *Appl. Phys. Lett.* 53, 640 (1988).
- Johns, S. T., Master Thesis, University of Arizona, (Tucson, 1991).
- Kawaguchi, H. and Kawamura, Y., *Electron Lett.* 23, 1013 (1987).
- Keyes, R. W., *Proc. IEEE* 69, 267 (1981).
- Khitrova, G., Iwabuchi, T., and Gibbs, H. M., *Superlattices and microstructures* 8, 439 (1990).
- Khitrova, G., Iwabuchi, T., Chuang, C. L., Yoon, T., Pon, R., and Gibbs, H. M., CMH2, CLEO'91, 1991 Technical Digest Series (Optical Society of America) 10, 54 (1991a).
- Khitrova, G., Iwabuchi, T., Chung, C. L., Yoon, T., and Gibbs, H. M., *J. Appl. Phys.*, to be published (1991b).
- Kittle, C., *Introduction to Solid State Physics* (John Wiley & Son, New York 1966).
- Knox, R. S., *Excitons*, (Academic Press, New York, 1963).
- Kuszelewicz, R., Sefz, B. G., Oudar, Michel, J. L., and Azoulay, R., *SPIE Proc.* 128, 209 (1990).
- Lee, S. G., Harten, P. A., Sokoloff, J. P., Jin, R., Fluegel, B., Meissner, K. E., Chuang, C. L., Binder, R., Koch, S. W., Khitrova, G. Gibbs, H. M., Polky, J. N., and Pubanz, G. A., *Phys. Rev. B* 43, 1719, (1991).
- Lobentanzer, H, Stolz, W., Ploog, K., Bauerle, R. J., and Elsaesser, T., *Solid State Electron.* 32, 1875 (1989).
- Park, S. H., Morhange, J. F., Jeffery, A. D., Morgan, R. A., Chavez-Prison, A., Gibbs, H. M., Koch, S. W., Peyghambarian, N., Derstine, M., Gossard, A. C., English, J. H., and Weigmann, W., *Appl. Phys. Lett.* 52, 1201 (1988).
- Pearsall, T. P., ed., *GAInAsP Alloy Semiconductors* (John Wiley & Sons, New York, 1982).
- Peyghambarian, N., Park, S. H., Koch, S. W., Jeffery, A., Potts, J. E., and Cheng, H., *Appl. Phys. Lett.* 52, 182 (1988).
- Tucker, R. S., Eisenstein, G., and Korotky, S. K., *J. of Light Tech.* 6, 1737 (1988).
- Schmitt-Rink, S., Chemla, D. S., and Miller, D. A. B., *Phys. Rev. B* 32, 6601 (1985).
- Senior, J. M., *Optical Fiber Communications* (Prentice-Hall International, Inc., London 1985).
- Sfez, B. G., Oudar, J. L., Michel, J. C., Kuselewicz, R., and Azoulay, R., *Appl. Phys. Lett.* 57, 324 (1990).
- Tackeuchi, A., Muto, S., Inata, T., and Fujii, T., *Appl. Phys. Lett.* 58, 15 (1991).
- Tai, K., Jewell, J. L., Tsang, W. T., Temkin, H., Panish, M., and Twu, Y., *Appl. Phys. Lett.* 50, 796 (1987).
- Weiner, J. S., Pearson, D. B., Miller, D. A. B., Chemla, D. S., Sivco, D., and Cho, A. Y., *Appl. Phys. Lett.* 49, 531 (1986).

**MISSION  
OF  
ROME LABORATORY**

*Rome Laboratory plans and executes an interdisciplinary program in research, development, test, and technology transition in support of Air Force Command, Control, Communications and Intelligence (C<sup>3</sup>I) activities for all Air Force platforms. It also executes selected acquisition programs in several areas of expertise. Technical and engineering support within areas of competence is provided to ESD Program Offices (POs) and other ESD elements to perform effective acquisition of C<sup>3</sup>I systems. In addition, Rome Laboratory's technology supports other AFSC Product Divisions, the Air Force user community, and other DOD and non-DOD agencies. Rome Laboratory maintains technical competence and research programs in areas including, but not limited to, communications, command and control, battle management, intelligence information processing, computational sciences and software producibility, wide area surveillance/sensors, signal processing, solid state sciences, photonics, electromagnetic technology, superconductivity, and electronic reliability/maintainability and testability.*